PROCEEDINGS OF SPIE

SPIEDigitalLibrary.org/conference-proceedings-of-spie

M-mode photoacoustic flow imaging

Hui Fang, Konstantin Maslov, Lihong V. Wang

Hui Fang, Konstantin Maslov, Lihong V. Wang, "M-mode photoacoustic flow imaging," Proc. SPIE 7177, Photons Plus Ultrasound: Imaging and Sensing 2009, 71772M (24 February 2009); doi: 10.1117/12.810159

SPIE.

Event: SPIE BiOS, 2009, San Jose, California, United States

M-mode Photoacoustic Flow Imaging

Hui Fang, Konstantin Maslov, and Lihong V. Wang*
Optical Imaging Laboratory, Department of Biomedical Engineering,
Washington University in St. Louis, St. Louis, Missouri 63130, USA

ABSTRACT

Recently, there has been a growing interest in the development of photoacoustic flow measuring methods aimed to study microvascular blood flow in deep tissue. Here, we describe a method of *M*-mode photoacoustic flow imaging, where a photoacoustic microscope equipped with a high repetition rate pulsed dye laser is used. As a demonstration, we studied the flow of a diluted suspension of carbon glassy particles in a small tube, and extracted the flow profile. Potentially, the method can be applied to detect the blood flow in microvessels either directly or by injecting optically absorbing particles.

Keywords: Photoacoustic imaging, *M*-mode imaging, flow measurement, flow profile

1. INTRODUCTION

Recently, photoacoustic imaging has progressed significantly [1] in studying microvascular structures as well as microvascular hemoglobin oxygen saturation, both in deep tissue. The progression lies in the unique properties of this imaging modality: the high optical absorption contrast from blood and the low scatting coefficient of ultrasound in biological tissue. For the same reason, we have also seen a growing interest in the development of photoacoustic flow measurements specifically aimed to study microvascular blood flow in deep tissue [2-5].

Although there exist several high-resolution optical blood flow measuring methods such as laser Doppler microscopy [6], Doppler optical coherent tomography [7], and laser speckle imaging [8], all of these pure optical methods have an imaging-depth limitation, which is less than 1 mm because of strong light scattering in tissue [9]. On the other hand, ultrasound imaging can image deep tissue but still faces a challenge to detect low speed blood flow in microvessels [10], mainly due to the very low contrast provided by the much weaker ultrasound scattering of red blood cells relative to that of surrounding tissue. A measuring method based on photoacoustic effect can alleviate these problems and provide a valuable tool.

Among a few reported photoacoustic flow measuring studies, those measurements [2,3] both applied nanoparticles to detect flow and both obtained the flow speed from changes in time dependent photoacoustic signal strength, and only an average flow speed was obtained and the flow profile was not discussed. The other experiments [4,5] demonstrated the continuous wave photoacoustic Doppler flow measurement, which can measure a flow profile from a complex theoretical model but can only detect the flow velocity component that is parallel to the ultrasonic detection axis. In this paper, we describe a pulsed photoacoustic flow measuring method, which is capable of obtaining directly a flow profile and also detecting a flow perpendicular to the ultrasonic detection axis.

2. *M*-MODE PHOTOACOUSTIC FLOW IMAGING

Similar to the terminology used in photoacoustic imaging such as "*A*-line" signals for depth profiling and "*B*-scan" images for cross sectional imaging [11], which are both analogous to those used in ultrasound imaging, we will call the new method "*M*-mode" photoacoustic flow imaging (MPFI)**.** The *M*-mode ultrasound is primarily used in echocardiography to detect cardiac motion [12] or to measure cardiac blood flow [13]. In *M*-mode imaging, multiple A-line

* lhwang@biomed.wustl.edu; phone: 314 935-6152; fax: 314 935-7448

Photons Plus Ultrasound: Imaging and Sensing 2009, edited by Alexander A. Oraevsky, Lihong V. Wang,
Proc. of SPIE Vol. 7177, 71772M · © 2009 SPIE · CCC code: 1605-7422/09/$18 · doi: 10.1117/12.810159

signals are recorded repeatedly along a fixed detection line and an image is displayed using time as the horizontal dimension and depth as the vertical dimension.

3. EXPERIMENTAL SYSTEM

Figure 1 plots the schematic of the system used to take an *M*-mode photoacoustic flow image. The system includes two subsystems where the major one is a dark-field reflection-mode photoacoustic microscope [14] and the other is a flow setup including a syringe pump, a Tygon tube (with an inner diameter of 0.25 mm and an outer diameter of 0.75 mm, S-54-HL, Saint-Gobain Performance Plastics), and a recycling container.

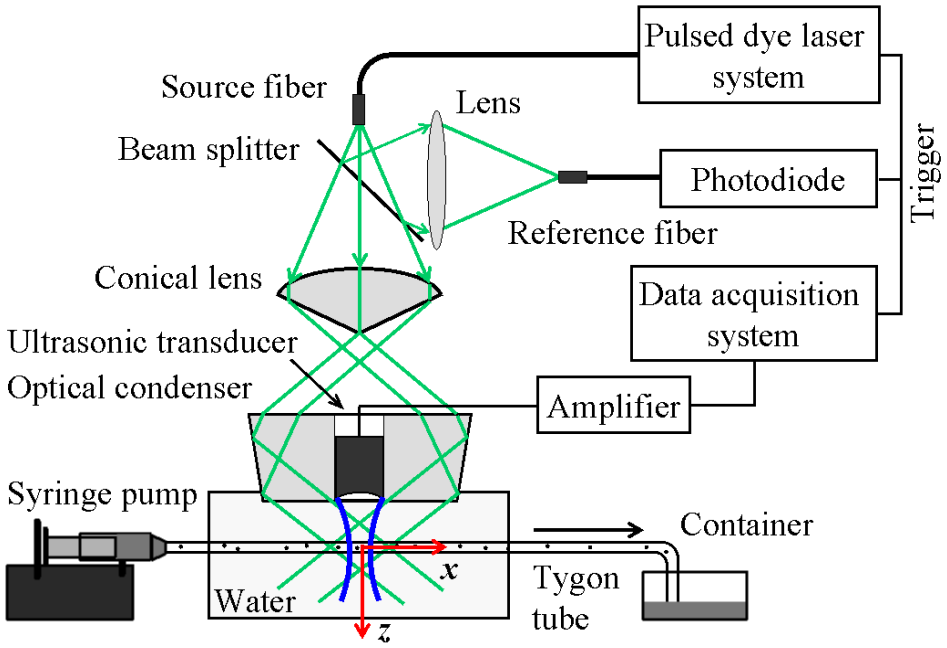

Fig. 1 Schematic diagram of the *M*-mode photoacoustic flow imaging system.

The photoacoustic microscope uses a conical lens and an optical condenser to form a dark field laser illumination pattern on the tissue surface, and uses an ultrasonic transducer to receive the photoacoustic signals. The current pulsed dye laser system has been upgraded from the previous one [11, 14, 15], now consisting of a Nd: YLF pump laser (INNOSLAB, EdgeWave) and a wavelength-tunable dye laser (Cobra, Sirah), which can provide laser pulses with a duration of 8 ns and a repetition frequency up to 5 kHz. For the experiment reported here, the pump laser was operated at a repetition frequency of 1 kHz and the dye laser was operated at 570 nm. The laser output optical fluence, measured near the tube surface, is about 12.1 mJ/cm^2. The laser is delivered through an optical fiber with a core diameter of 1 mm, and the reflected laser beam is collected by another optical fiber with a core diameter of 105 μm and subsequently detected by a photodiode as a reference signal. We used a spherically focused ultrasonic transducer (V212-BB-RM, Panametrics), which has an actual center frequency of 22 MHz, a nominal bandwidth of 80%, and a numerical aperture (NA) of 0.6. The output from the transducer was amplified 24 dB by a low-noise, wideband amplifier (Mini-Circuits) and was then digitized at a 200 MHz sampling rate by a 14 bit data acquisition system (GaGe, Inc.). The photoacoustic microscope can perform three-directional scans by a motorized translation stage.

A diluted suspension of carbon glassy spherical powder, with particle size distributed from 2 to 12 micrometers (484164, Sigma-Aldrich) and with a volume fraction of particles $\phi = 0.1\%$, was studied. The Tygon tube was laid horizontally (i.e., perpendicularly to the axis of the ultrasonic transducer) inside a water tank. The flow measurement was taken at a distance of 50 cm from the tube entrance. Before the measurement, the photoacoustic microscope was aligned and focused onto the tube center.

4. *M*-MODE PHOTOACOUSTIC FLOW IMAGE

Figure 2 displays a typical *M*-mode photoacoustic image for the flow with an average flow speed of 4.40 mm/s. The image in Fig. 2(a) has a pixel dimension of 250×200, where 250 is the number of time points and 200 is the number of depth points. Here, the depth, *z*, is calculated from the A-line sampling rate 200 MHz and the speed of sound 1.50×10^3 m/s in water. The location of $z = 0$ is set to the position of the transducer focus. In the image, several bright horizontal bars can be clearly visualized. They are the traces of individual carbon particles that passed through the transducer's focal zone as shown in Fig. 1 (because of the low particle volume fraction). As an example, Fig. 2(b) plots the pressure amplitude signal taken along the line of $z = 0$, which shows one of the traces. Since these traces contain information about both the transit time and the width of the transducer's focal zone, the flow speed can be obtained with the following data processing model.

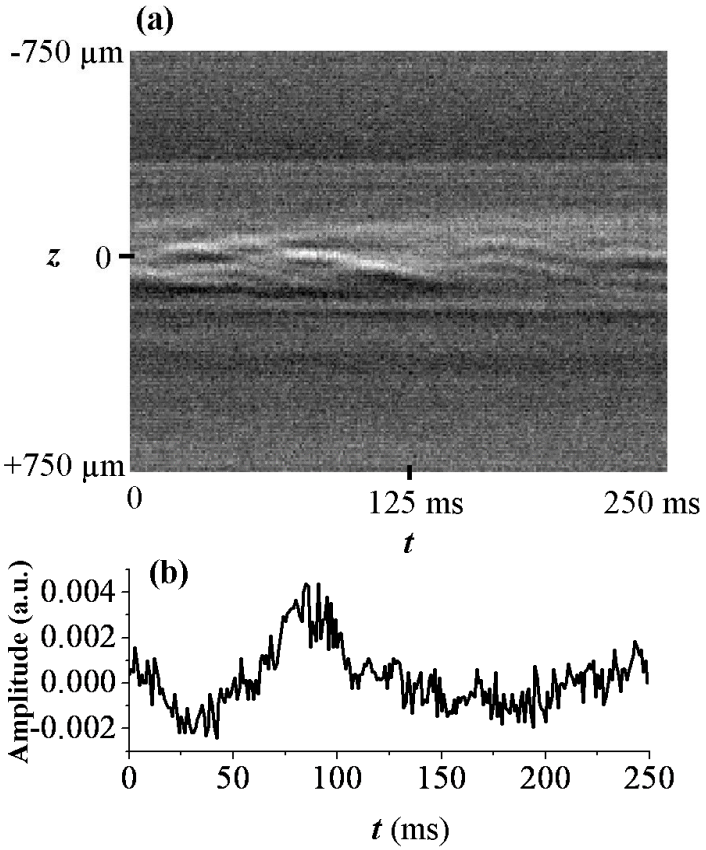

Fig. 2 An *M*-mode photoacoustic image for a flow of a carbon particle suspension inside a small tube. The flow has an average flow speed of 4.40 mm/s. (a) The image, which has pixel dimensions of 250×200, 250 in *t* and 200 in *z*. (b) The pressure amplitude signal taken from the image along the line of $z = 0$.

5. THEORETICAL MODEL TO EXTRACT FLOW SPEED

We consider a simplified model, assuming that the ultrasonic transducer has a Gaussian pressure sensitivity profile [16] on any z plane inside the focal zone as

$$P_z(x,y) = A(z) \times \exp[-\frac{(x-x_0)^2 + (y-y_0)^2}{2 \cdot R(z)^2}], \quad (1)$$

where $A(z)$ denotes the peak pressure sensitivity at depth z, x_0 and y_0 denote the lateral displacement from the transducer axis, and $R(z)$ represents the $1/e^{1/2}$ half width of the profile at depth z. $R(z)$ can be estimated directly in the spatial domain by scanning a thin carbon fiber perpendicular to the ultrasonic axis. In an M-mode photoacoustic flow image such as the one shown in Fig. 2, $R(z)$ is reflected indirectly in the time domain by a particle moving along the flow path.

In Fig. 2, we can define the x axis along the flow direction. The motion of a particle correlates the location and the time according to

$$(x - x_0) = v(z) \cdot (t - t_0), \quad (2)$$

where $v(z)$ is the particle's moving speed (also the flow speed) at z, and t_0 is the moment when the particle passes the $x = x_0$ line on the z plane. Because of Eq. (2), the sensitivity profile in Eq. (1) can be written in the time domain as

$$P_z(t,y) = A(z) \times \exp[-\frac{(y-y_0)^2}{2 \cdot R(z)^2}] \times \exp[-\frac{(t-t_0)^2}{2 \cdot T(z)^2}], \quad (3)$$

where we defined $T(z)$ according to

$$v(z) = \frac{R(z)}{T(z)}. \quad (4)$$

Therefore, $v(z)$ can be obtained by measuring both $R(z)$ and $T(z)$.

In principle, we can measure $T(z)$ from an individual particle as shown in Fig. 2(b). However, to get more accurate results of $T(z)$, we used another approach. We first took an M-mode photoacoustic image over a sufficient period of time, and we then calculated the autocorrelations of one-dimensional signals taken from the image at every z. As a result, we obtained the average autocorrelation of the sensitivity profiles expressed in Eq. (3) from many individual particles:

$$C(\tau, z) = < P_z(t,y) \otimes P_z(t,y) > = B \times \exp[-\frac{\tau^2}{4 \cdot T(z)^2}], \quad (5)$$

where B does not depend on τ and y. Here, we assume that the data of different particles in the M-mode image do not overlap.

6. FLOW MEASURING RESUTLS

6.1 Point Spread Function of the Photoacoustic Microscope

We started with the experiment of scanning a 6-μm-diameter carbon fiber near the focal zone of the transducer to obtain $R(z)$. The carbon fiber was aligned along the y axis and was scanned on the x-z plane with step sizes of 2.5 μm along x and 2.0 μm along z. Figure 3(a) displays the scanning photoacoustic image. As examples, Figs. 3(b) and 3(c) show respectively two pressure amplitude signals taken from the image in Fig. 3(a) at $z = 0$ and $z = -240$ μm. The solid lines in both figures plot the Gaussian fits. Figure 3(d) plots the $R(z)$ extracted from the Gaussian fits of the data

shown in Figs. 3(b) and 3(c), and plots the further smoothed results as the solid line. The value of the solid line will be used as $R(z)$ to calculate $v(z)$ according to Eq. (4).

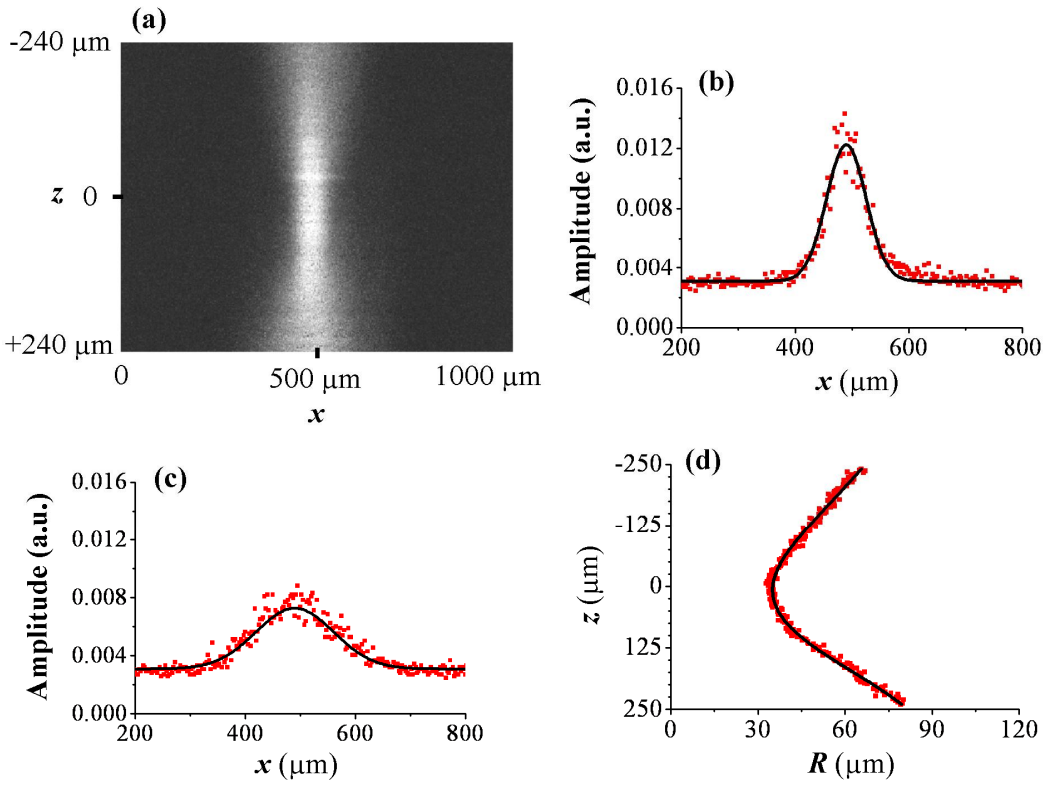

Fig. 3 Procedure to obtain the $R(z)$ from the photoacoustic image by scanning a 6-μm-diameter carbon fiber on the *x*-*z* plane near the focal zone of the transducer. (a) The scanning photoacoustic image on the *x*-*z* plane. (b) Pressure sensitivity profiles taken from (a) at $z = 0$. (c) Pressure sensitivity profiles taken from (a) at $z = -240\ \mu\text{m}$. The solid lines in both (b) and (c) plot the Gaussian fits. (d) The $R(z)$. The data points plot the results of the Gaussian fits of the data in (b) and (c) and the solid line plots the smoothed result.

6.2 Flow Profile

We then took the M-mode photoacoustic flow images for three flows with different average speeds of $v_1 = 1.10$ mm/s, $v_2 = 2.20$ mm/s, and $v_3 = 4.40$ mm/s. The total time for taking each image is 20 seconds. Therefore, there are a total of 20,000 data points in the horizontal dimension of each image. Next, we performed the autocorrelation calculation. As examples, Figs. 4(a) and 4(b) plot the resulted autocorrelations of the signals taken from the center of the tube at $z = 0$ and from the edge of the tube at $z \approx +125\ \mu\text{m}$, respectively. The data points plot the computed autocorrelation and the solid lines plot the corresponding Gaussian fits based on Eq. (5). Because the signal level is lower at $z \approx +125\ \mu\text{m}$ than that at $z = 0$, the autocorrelation data points in Fig. 4(b) are noisier. Also, because the focal zone is wider at $z \approx +125\ \mu\text{m}$ than that at $z = 0$ even if the flow speeds are equal, the autocorrelations in Fig. 4(b) are broader. From the autocorrelation Gaussian fits, we obtained $T(z)$.

Finally, we calculated the flow speeds with Eq. (4) and the results are plotted as data points in Fig. 4(c). For comparison, the solid lines plot the anticipated preset average flow speeds v_1, v_2, and v_3. As can be seen, the extracted flow profiles are approximately flat. The flat profile corresponds to the results reported in [17], where a similar flow setup was used. The measured flow speeds are also in good agreement with the anticipated values of v_1, v_2, and v_3, with maximum relative errors of 16.3%, 13.5%, and 8.9%, respectively.

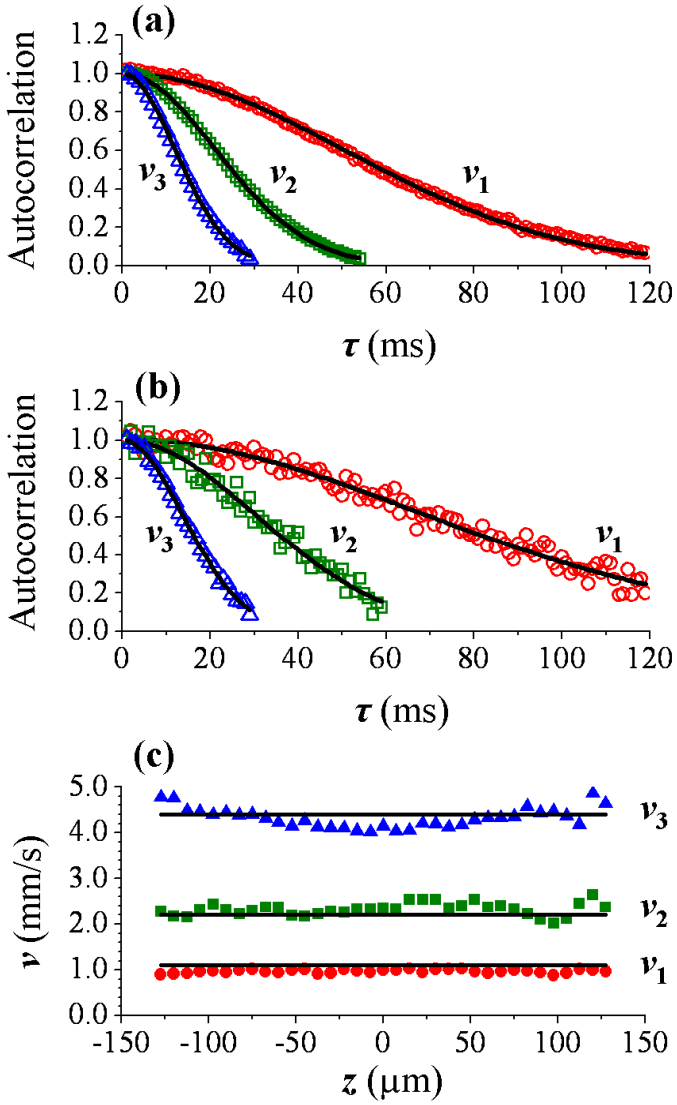

Fig. 4 Autocorrelations and extracted flow speeds for three flows with the average speeds of $v_1 = 1.10$ mm/s, $v_2 = 2.20$ mm/s, and $v_3 = 4.40$ mm/s. (a) Autocorrelations at $z = 0$, the center of the small tube. (b) Autocorrelations at $z \approx +125$ μm, the edge of the small tube. In both (a) and (b), the data points plot the experimental data and the solid lines plot the Gaussian fits. (c) Extracted flow speed profiles (plotted as data points) and the preset average flow speeds v_1, v_2, and v_3 (plotted as solid lines).

7. DISCUSSION AND FUTURE WORK

In this study, we have demonstrated the MPFI with a diluted carbon particle suspension, by the experiment performed in clear media with the best possible signal-to-noise ratio, and for the flow perpendicular to the ultrasonic axis. Since our major goal is to measure the mcirovacular blood flow in tissue, we will extend the MPFI study for the flow in scattering media and with other directions.

If we do the Gaussian fitting using Eq. (3) for the single particle trace in Fig. 2(b) that corresponds to v_3 at $z = 0$, we obtained $T(0) = 10.0$ ms. Since $R(0) = 35.2$ μm, from Eq. (4), we obtain $v_3(0) = 3.5$ mm/s, which underestimates the preset value of 4.40 mm/s by 20%. Therefore, it is more accurate to extract the flow speed by using the autocorrelation approach. The accuracy can be improved further by increasing the laser pulse repetition rate, resulting in an increase of the number of data points in the autocorrelation window.

The accuracy in the present study is also limited by the large focal spot size which is comparable to the small tube, especially for the flow speed measured near the tube center where the flow speed could have a large distribution along the lateral direction. Decreasing the focal spot size can improve the accuracy. We are working on the MPFI experiment with the optical resolution photoacoustic microscope [18], where the lateral resolution approaches the size of a single red blood cell.

Potentially, the MPFI can be applied to detect microvascular blood flow in tissue by injecting exogenous photoacoustic contrast particles in low concentration. With the improvement in lateral resolution, it becomes feasible to apply the MPFI to measure the blood flow in a capillary noninvasively by using endogenous contrast provided by red blood cells.

ACKNOWLEDGEMENT

We acknowledge the support provided by National Institutes of Health under grants R01 EB000712 and R01 NS046214. We thank Song Hu and Erich Stein for the useful discussion.

REFERENCES

[1] L. V. Wang, "Tutorial on photoacoustic microscopy and computed tomography," IEEE. J. Sel. Top. Quantum Electron. **14**, 171-179 (2008).
[2] P. C. Li, S. W. Huang, and W. W. Chen, "Photoacoustic flow measurements by use of laser-induced shape transitions of gold nanorods," Opt. Lett. **30**, 3341-3343 (2005).
[3] W. W. Chen, C. K. Liao, H. C. Tseng, Y. P. Lin, C. C. Chen, and P. C. Li, "Photoacoustic flow measurements with gold nanoparticles," IEEE Trans. Ultrason., Ferroelect., Freq. Contr. **53**, 1955-1959 (2006).
[4] H. Fang, K. Maslov, and L. V. Wang, "Photoacoustic Doppler effect from flowing small light-absorbing particles," Phys. Rev. Lett. **99**, 184501-(1-4) (2007).
[5] H. Fang, K. Maslov, and L. V. Wang, "Photoacoustic Doppler flow measurement in optically scattering media," Appl. Phys. Lett. **91**, 264103-(1-3) (2007).
[6] M. Atlan, B. C. Forget, A. C. Boccara, T. Vitalis, A. Rancillac, A. K. Dunn, and M. Gross, "Cortical blood flow assessment with frequency-domain laser Doppler microscopy," J. Biomed. Opt. **12**, 024019-(1-8) (2007).
[7] Y. W, B. A. Bower, J. A. Izatt, O. Tan, and D. Huang, "*In vivo* total retinal blood flow measurement by Fourier domain Doppler optical coherence tomography," J. Biomed. Opt. **12**, 041215-(1-8) (2007).
[8] P. Li, S. Ni, L. Zhang, S. Zeng, and Q. Luo, "Imaging cerebral blood flow through the intact rat skull with temporal laser speckle imaging," Opt. Lett. **31**, 1824-1826 (2006).
[9] R. Bonner and R. Nossa, "Model for laser Doppler measurements of blood flow," Appl. Opt. **20**, 2097-2107 (1981).
[10] D. E. Goertz, J. L. Yu, R. S. Kerbel, P. N. Burns, and F. S. Foster, "High-frequency 3-d color-flow imaging of the microcirculation," Ultrasound in Med. & Biol. **29**, 39-51 (2003).

[11] H. F. Zhang, K. Maslov, and L. V. Wang, "*In vivo* imaging of subcutaneous structures using functional photoacoustic microscopy," Nat. Protocols **2**, 797-804 (2007).
[12] S. I. Rabben, A. H. Torp, A. Stoylen, S. Slordahl, K. Bjornstad, B. O. Haugen, and B. Angelsen, "Semiautomatic contour detection in ultrasound M-mode images," Ultrasound in Med. & Biol. **26**, 287-296 (2000).
[13] M. J. Garcia, D. Thomas and A. L. Klein, "New Doppler echocardiographic applications for the study of diastolic function," J. Am. Coll. Cardiol. **32**, 865-875 (1998).
[14] K. Maslov, G. Stoica, and Lihong V. Wang, "*In vivo* dark-field reflection-mode photoacoustic microscopy," Opt. Lett. **30**, 625-627 (2005).
[15] H. F. Zhang, K. Maslov, G. Stoica and L. V. Wang, "Functional photoacoustic microscopy for high-resolution and noninvasive *in vivo* imaging," Nat. Biotechnol. **24**, 848-851 (2006).
[16] R. O. Claus and P. S. Zerwekh, "Ultrasonic transducer with a two-dimensional Gaussian field profile," IEEE Trans. Sonics Ultrason. **30**, 36-39 (1983).
[17] A. Sourice, G. Plantier, and J. L. Saumet, "Red blood cell velocity estimation in microvessels using the spatiotemproral autocorrelation," Meas. Sci. Technol. **16**, 2229-2239 (2005).
[18] K. Maslov, H. F. Zhang, S. Hu, and L. V. Wang, "Optical-resolution photoacoustic microscopy for *in vivo* imaging of single capillaries," Opt. Lett. **33**, 929-931 (2008).